DMD Fast Forward. Published on December 19, 2018 as DOI: 10.1124/dmd.118.083766
This article has not been copyedited and formatted. The final version may differ from this version.

TITLE PAGE

KINETICS OF CYCLOPHOSPHAMIDE METABOLISM IN HUMAN, DOG, CAT, AND MOUSE AND RELATIONSHIP TO CYTOTOXIC ACTIVITY AND PHARMACOKINETICS

Dominique A. Ramirez, Keagan P. Collins, Allister E. Aradi, Katherine A. Conger and Daniel L. Gustafson

Department of Clinical Sciences (D.A.R., A.E.A., D.L.G.) and School of Biomedical Engineering (K.P.C., K.A.C., D.L.G.), Colorado State University, Fort Collins, Colorado; and University of Colorado Cancer Center (D.L.G.), Aurora, Colorado.

RUNNING TITLE PAGE

COMPARATIVE KINETICS OF CYCLOPHOSPHAMIDE METABOLISM

Corresponding Author:

Dominique A. Ramirez; Phone: 970.297.4057; Email: mando.ramirez@colostate.edu

Address: Robert and Mary Flint Animal Cancer Center, 1620 Campus Delivery, 300 W Drake Road, Fort Collins, CO, 80523

Number of text pages: 47

Number of tables: 4

Number of figures: 7

Number of references: 58

Number of words in ABSTRACT: 228

Number of words in INTRODUCTION: 698

Number of words in DISCUSSION: 1450

Abbreviations:

CP, cyclophosphamide; 4OHCP, 4-hydroxycyclophosphamide; 4OHCP-SCZ, 4-hydroxycyclophosphamide semicarbazone; PM, phosphoramide mustard; CL_{int}, intrinsic clearance; AUC, area under the curve; PK, pharmacokinetics; CYP, cytochrome P450; H, human; D, dog; C, cat; M, mouse; CBP, 4-(4-chlorobenzyl)-pyridine

DMD Fast Forward. Published on December 19, 2018 as DOI: 10.1124/dmd.118.083766
This article has not been copyedited and formatted. The final version may differ from this version.

ABSTRACT

Cyclophosphamide (CP), a prodrug that is enzymatically converted to the cytotoxic 4-hydroxycyclophosphamide (4OHCP) by hepatic enzymes, is commonly used in both human and veterinary medicine to treat cancers and modulate the immune system. The metabolism of CP in humans, dogs, cats, and mice was investigated with liver microsomes and apparent K_M, V_{max}, and intrinsic clearance (V_{max}/K_M,) parameters were estimated. The inter- and intra-species variation in kinetics was vast. Dog microsomes were, on average, 55-fold more efficient than human microsomes, 2.8-fold more efficient than cat microsomes, and 1.2-fold more efficient than mouse microsomes at catalyzing CP bioactivation. These differences translated to cell-based systems. Breast cancer cells exposed to 4OHCP via CP bioactivation by microsomes resulted in a stratification of cytotoxicity dependent on the species of microsomes measured by IC₅₀: dog (31.65 μM), mouse (44.95 μM), cat (272.6 μM), and human (1857 μM). The contribution of cytochrome P450s (CYP), specifically CYP2B, CYP2C, and CYP3A to CP bioactivation were examined: CYP3A inhibition resulted in no change in 4OHCP formation; CYP2B inhibition slightly reduced 4OHCP in humans, cats, and mice; and CYP2C inhibition drastically reduced 4OHCP formation in each species. Semi-physiologic modeling of CP metabolism using scaled metabolic parameters resulted in simulated data that closely matched published pharmacokinetic (PK) profiles, determined by non-compartmental analysis. The results highlight differential CP metabolism delineated by species and demonstrate the importance of metabolism on CP clearance.

DMD Fast Forward. Published on December 19, 2018 as DOI: 10.1124/dmd.118.083766
This article has not been copyedited and formatted. The final version may differ from this version.

INTRODUCTION

Cyclophosphamide (CP) is an oxazaphosphorine antineoplastic agent used to treat a variety of hematopoietic and solid tumors both in human and veterinary medicine. It is also used as an immunosuppressant for some autoimmune diseases and for immunoablation in bone marrow transplants (Ahmed and Hombal, 1984, Emadi et al., 2009). CP can be dosed intravenously or orally following a variety of schedules depending on the application. Typical chemotherapeutic doses in humans are 500-1200 mg/m^2 cumulatively when administered every 21 days either as a single dose or fractionated over multiple doses (de Jonge et al., 2005, Penel et al., 2012). Chemotherapeutic doses of CP in dogs and cats range from 200-250 mg/m^2 (Garrett et al., 2002, Warry et al., 2011) and 200-300 mg/m^2 (Teske et al., 2002, Stroda et al., 2017), respectively, and are reflective of the UW-Madison protocol and its variations. The doses used in humans, dogs, and cats are empirically determined from the maximum tolerated dose in each of the species with sparse historical pharmacokinetic data available for comparison due to the complex nature of CP pharmacology. CP, a pro-drug, requires metabolic activation to 4-hydroxycyclophosphamide (4OHCP) for initiation of a spontaneous breakdown cascade (Figure 1) resulting in the generation of the putative cytotoxic phosphoramide mustard (PM) capable of bifunctional alkylation (Groehler et al., 2016) and acrolein, which causes varying degrees of bladder toxicity (Moghe et al., 2015). The conversion of CP to 4OHCP is believed to happen only in the liver, as opposed to occurring directly in cancer cells (Boddy and Yule, 2000), and the production of 4OHCP is dependent on hepatic enzymes, namely the cytochrome P450 (CYP) superfamily (Bagley et al., 1973, Li et al., 2010).

The complex sequelae associated with hepatic production of reactive metabolites that must traverse from the liver through the blood to target tumor cells for antineoplastic activity, or normal tissues for toxicity, have made pharmacokinetic-pharmacodynamic relationships for CP difficult to define. Early *in vitro* cytotoxicity bioassays relied on treating cells with plasma from humans or animals dosed with CP (Stevenson and Fauci, 1980). Following improvements in

chemical synthesis and liver microsome isolation methods, contemporary scientists studying CP *in vitro* have the option of using other bioactivation strategies or commercially available PM precursors, such as the peroxide 4-hydroperoxycyclophosphamide, that don't require enzymatic activation. Additionally, improvements in techniques that trap transient metabolic intermediates have permitted better and more sensitive quantification of CP from biological matrices (Huitema et al., 2000).

Recently, in concordance with improved methods for liver microsome isolation and supersome production, human-oriented CP research has identified important molecular components responsible for CP metabolism (Roy et al., 1999, Huang et al., 2000, Kumar et al., 2007). In humans, these proteins are known to vary widely between individuals on an expression and polymorphism basis (Zanger and Schwab, 2013). A number of human CYP isoforms have been implicated in the bioactivation of CP, namely CYP2B6, CYP3A4, CYP2C9, and CYP2C19 (Rodriguez-Antona and Ingelman-Sundberg, 2006), but CYP2B6 is hypothesized to be the putative critical enzyme responsible for 4OHCP formation (Xie et al., 2003). These studies complement the growing canon of CP research in humans that includes *in vitro*, *in vivo*, and pharmacokinetic (PK) work. In contrast, most published CP-related research in the veterinary field is clinical, and a gap persists in pharmacologic and molecular knowledge. Because animal surrogates for human cancers are vital translational models for cancer research and pharmacology, animal cancer research is equally key for the progression of clinical veterinary medicine and improving comparative oncology, even for a drug as well-established in the clinic as CP.

In the present study, steady-state kinetics of CP bioactivation by hepatic microsomes were investigated in three species frequently treated with CP – humans, dogs, and cats – and in the traditional preclinical animal model, the mouse. These data identified significant metabolic differences between the species' apparent kinetic parameters K_M and V_{max}. *In vitro* application of these data revealed predictable cytotoxic responses dependent on the kinetics of CP activation.

Using these data *in silico* to retrospectively compare prior CP PK data to those simulated based purely on scaled metabolic parameters suggests that hepatic CP activation coupled with liver blood flow and protein binding primarily drives CP clearance in humans, dogs, cats, and mice.

MATERIALS AND METHODS

Chemicals

Cyclophosphamide monohydrate, hexamethylphosphoramide, semicarbizide hydrochloride, sulfaphenazole, and anhydrous EDTA were purchased from Sigma-Aldrich (St. Louis, MO). 4-hydroperoxycyclophosphamide, a precursor to 4-hydroxycyclophosphamide, was purchased from Niomech-IIT (Bielefeld GmbH, Germany). 4-(4-chlorobenzyl)pyridine and fluconazole were purchased from TCI Chemicals (Portland, OR). Miconazole and chloramphenicol were purchased from MP Biomedicals (Solon, OH). Ketoconazole was purchased from Acros Organics (New Jersey). β-NADPH tetrasodium salt was purchased from Roche Life Science (Indianapolis, IN). Gentest™ NADPH Regenerating System components were purchased from Corning (Corning, NY). Potassium phosphate dibasic anhydrous, potassium phosphate monobasic, and molecular grade D-sucrose were purchased from Fisher Scientific (Waltham, MA). Acetonitrile and other solvents used for LC-MS/MS are of UPLC/MS grade and were purchased from Fisher Scientific (Waltham, MA).

Microsome Sources and Preparation

Microsomes used in this study include commercially available and freshly isolated batches. Source information for microsomes used in this study is listed in Table 1. Isolated microsomes were prepared by differential centrifugation from liver samples either from freshly harvested liver sections, or from liver samples that had been stored frozen at -80°C. Freshly harvested liver sections were kept on ice for immediate microsome processing. Liver pieces that had to be frozen were kept below 25°C, on ice, until they could be transferred into tubes for storage at -80°C and were not thawed until microsome isolation. Storage of liver at -80°C has been shown not to result in loss of P450 in liver samples (Yamazaki et al., 1997). All steps of the isolation were performed at 4°C or on ice. Liver sections were first homogenized in homogenization buffer (HB: 100mM D-sucrose, 1mM EDTA) with a dounce homogenizer fitted to a handheld power drill at a 100 mg-liver-weight/mL HB ratio. Homogenates were subjected to

the following differential centrifugation scheme: 800x*g* for 10 minutes, 7,000x*g* for 10 minutes, and 18,000x*g* for 5 minutes. After each spin, the supernatant was transferred to a new centrifuge tube and the pellet was discarded. After the 18,000x*g* spin, the supernatant was spun at 100,000x*g* for one hour. The supernatant was discarded and the pellet containing microsomes was resuspended gently in HB in a volume ranging from 100–400µL. Microsomes were then stored at -80°C and an aliquot was used to determine total protein concentration via the BCA assay, in duplicate (Thermo Scientific, Waltham, MA). Microsome aliquots were thawed on ice for incubation and kinetics experiments and were not used after three freeze/thaw cycles, in line with published data on CYP stability (Pearce et al., 1996).

Microsome Incubations

Microsomes were incubated to determine optimal reaction conditions (concentration of microsomal protein and incubation time) for downstream kinetics assays. Reactions were prepared with microsomes (0.5 mg/mL) and 1.0 mM NADPH (solvated in 0.1 M phosphate buffer) in 0.1 M phosphate buffer (44mM KH_2PO_4, 56 mM K_2HPO_4, pH 7.4 and adjusted with NaOH). A reaction master mix was prepared without substrate and pre-incubated at 37°C for 5 minutes, and was then initiated by the addition of substrate (2 µg/mL CP) and incubated at 37°C. At specific time points (0, 5, 10, 20, 30, 45, 60) 100µL of sample was removed from the master mix and stopped with an equal volume of acetonitrile and chilled on wet ice, and 2M semicarbizide hydrochloride (SCZ) (1:10 dilution into sample, final ~0.2M) was immediately added to trap 4OHCP (4OHCP-SCZ) and prevent spontaneous breakdown (Warry et al., 2011). Samples were either frozen for later use or prepared immediately for LC/MS analysis. It has been shown that storage at -80°C for up to 12 months after semicarbizide trapping does not affect the stability of the 4OHCP metabolite (Huitema et al., 2000). Each incubation was performed in technical singlet. Protein concentration was increased to 1.0 mg/mL and the incubations were repeated if insignificant 4OHCP formation was observed at 0.5 mg/mL.

Michaelis-Menten kinetic assays were performed by incubating microsomes with cyclophosphamide using a discontinuous methodology. Individual reactions at each CP concentration were performed as technical singlets. Reactions were prepared with microsomes with a NADPH Regenerating System (ensuring ~1.3 mM NADPH) in 0.1 M phosphate buffer. Reactions were prepared without substrate and pre-incubated at 37°C for 5 minutes. Reactions were initiated by the addition of substrate and incubated at 37°C for the duration of the reaction. Reaction times and specific microsome concentrations for each species, determined from incubations described above, used for kinetics experiments are as follows: human (20 minutes, 1.0 mg/mL protein); dog (5 minutes, 0.5 mg/mL protein); cat (10 minutes, 0.5 mg/mL protein); and mouse (5 minutes, 0.5 mg/mL protein). These conditions were chosen as they demonstrated linear product formation with respect to time (data not shown). Reactions were stopped using the same method as described above. Samples were then either frozen for later analysis or prepared immediately for LC-MS/MS.

We selected 0.5 mg/mL microsomal protein as the optimal starting concentration for our incubations in accordance with published methods and guidelines for performing enzyme kinetics assays (Jia and Liu, 2007, Vrbanac and Slauter, 2013). Two different sources of NADPH were used as described above depending on the type of assay. Stability tests performed in-house suggest that NADPH is unstable but is usable in incubations for up to 30 minutes at 37°C in water and phosphate buffer (data not shown). In assays that did not require lengthy incubations, such as the discontinuous kinetics assays, NADPH salt was used. For assays that required incubation times up to and beyond 30 minutes, the regenerating system was employed.

Cytochrome P450 Inhibition Assays

Microsomes were incubated with CP and different CYP inhibitors to determine the contribution of certain CYP isozymes in the metabolism of CP. The following inhibitors were used at the listed concentrations: 4-(4-chlorobenzyl)pyridine (CBP) at 1 μM targeting CYP2B6

(Korhonen et al., 2007); ketoconazole at 1 μM targeting CYP3A4 (Eagling et al., 1998, Kuroha et al., 2002); fluconazole at 25 μM targeting CYP2C9 (Back et al., 1988, Miners and Birkett, 1998); and miconazole at 1 μM targeting CYP2C19 (Niwa et al., 2005). Importantly, fluconazole can also inhibit CYP3A4 (Kunze et al., 1996), similar to miconazole (Sakaeda et al., 2005). Additionally, chloramphenicol at 10 μM targeting canine CYP2B11 and sulfaphenazole at 100 μM targeting canine CYP2C21/41 have been identified (Perez Jimenez et al., 2018) and were included for the dog microsome only. The concentrations selected are higher than published IC_{50} to ensure sufficient inhibition of respective CYPs. Inhibitors were prepared in methanol but were diluted in phosphate buffer such that the organic concentration would be < 1% after final addition into reaction mixtures.

Reaction master mixes were prepared with microsomes, a NADPH Regenerating System (ensuring ~1.3 mM NADPH), 0.5 mg/mL microsomal protein, and inhibitor in 0.1 M phosphate buffer. Reactions were pre-incubated at 37°C for 10 minutes to account for any mechanism based inactivation of CYPs. Reactions were initiated with addition of 2 μg/mL CP and at specified time points (0, 5, 10, 15, 30, 60, 90, 120 minutes) 100 μL was removed and the reaction was stopped using the same method as described above. Samples were then either frozen or prepared immediately for analysis of 4OHCP and CP by LC-MS/MS. Inhibition experiments as described were done in singlet. Quantified 4OHCP concentration (μM) at every time point, for each condition, was normalized to the initial quantified CP concentration (μM) and plotted. Area under the curve (AUC) for each normalized 4OHCP vs time curve was calculated using the trapezoidal method implemented in GraphPad Prism 7.0d (GraphPad Software Inc., La Jolla, CA). AUC from each condition was then normalized again, this time to the control condition (microsomes with CP only, labeled “+CP”).

LC-MS/MS Analysis

Samples were processed for analysis via LC-MS/MS by a modification of a previously described method (Warry et al., 2011). In cases where substrate exceeded 100 μg/mL, samples

were diluted by a factor of 100. Dilution quality controls were used to validate the dilutions as analytically appropriate. Samples for LC-MS/MS analysis were prepared fresh or were thawed if frozen. Hexamethylphosphoramide (HMP, internal standard) was spiked into each sample at a final concentration of 500 ng/mL and samples were vortexed for 5 minutes. Samples were centrifuged at 20,000x*g* for 5 minutes and the supernatant was collected for analysis. Positive ion electrospray ionization mass spectra were obtained with an Applied Biosystems SCIEX 3200 QTRAP (SCIEX LLC, Framingham, MA) triple quadrupole mass spectrometer with a TurboIonSpray source interfaced to a Shimadzu Prominence HPLC system (Shimadzu Scientific Instruments Inc., Columbia, MD) and a CTC Analytics HTC PAL System autosampler (CTC Analytics, Lake Elmo, MN). Samples were chromatographed with a Waters SunFire C18 5 µm, 4.6x50 mm column (Waters Corp., Milford, MA) protected by a Security-Guard C18 cartridge (Phenomenex, Torrence, CA). Ammonium acetate (10 mM, pH 8.0, adjusted with NH_4OH) was solvent A, and acetonitrile was solvent B. Chromatographic separation was accomplished in six minutes at a flow rate of 440 µL/min using the following gradient: minute 0.0, 10% B; minute 1.0, 10% B; minute 3.0, 60% B; minute 4.0, 60% B; minute 4.5, 10% B. Analytes were quantified via multiple reaction monitoring of the ion transitions for 4OHCP-SCZ, CP, and HMP. Nitrogen gas was used as the collision gas. Three ion transitions for 4OHCP-SCZ were monitored and summed into one peak for analysis: *m/z* 334.3 -> 221.3, *m/z* 334.3 -> 259.3, and *m/z* 334.3 -> 114.3. These three peaks were incorporated into the final method, as opposed to using a single transition, as the sum of these three peaks greatly improved sensitivity and detection of 4OHCP from biological matrices. CP was monitored as *m/z* 261.2 -> 140.2. HMP was monitored as *m/z* 180.0 -> 135.0. The chromatographic peaks associated with 4OHCP-SCZ, CP, and HMP were integrated and the concentrations of the samples were based on the ratio of analyte:internal standard using Analyst® (AB SCIEX LLC, Framingham, MA) software.

Kinetics Analysis

Michaelis-Menten parameters were determined for each microsome source following incubations (listed above), performed in singlet. Formation of product (4OHCP-SCZ) was determined absolutely with LC-MS/MS and converted to velocity (pmol 4OHCP/min/mg-protein). GraphPad Prism 7.0d analysis software was used to estimate the Michaelis-Menten parameters. Specific CP concentrations used to estimate the kinetic parameters varied between microsome batches, but in no case were any data points excluded from the Michaelis-Menten curves. Velocity-substrate data were transformed using Eadie-Hoftsee linearization to assess the quality of the experiments, where the case of non-linearity suggests poor experimental design, execution, and/or a multiple enzyme model (Supplemental Figure 1).

Cell Culture

MDA-MB-231 human mammary epithelial tumor cells were purchased from ATCC (Manassas, CA) and maintained in Ham's F-12 Modified Media (Corning 10-080-CV, Corning, NY) supplemented with 10% FBS, 1 mM sodium pyruvate, 100 units of penicillin, and 100 µg/mL streptomycin and grown at 37°C and 5% CO_2. Cells were verified to be mycoplasma-free via PCR (Uphoff and Drexler, 2013) prior to transduction with IncuCyte® NucLight Red lentiviral system (Essen BioScience Inc., Ann Arbor, MI) under puromycin selection to stably express nuclear-localized red fluorescent protein.

Cytotoxicity Assays

NucLight Red labeled MDA-MB-231 cells were plated into 96-well plates in supplemented Ham's F-12 media at a density to ensure mid/late-log phase growth between 72-76 hours after plating. Cells were treated with microsomes and cyclophosphamide to mimic *in vivo* metabolism of CP to its active metabolite. Two different controls were tested in the development of the cytotoxicity assay, one being cells exposed neither to CP nor microsomes, and the second being cells exposed to microsomes but not CP for the duration of the experiment. The first control verified there were no volatile metabolites formed during the assay that could contaminate other wells (data not shown), and thus for each subsequent assay only

the second control was used. Reaction mixtures containing microsomes (1.0 mg/mL), CP (3.8 – 3831 μM), and a NADPH regenerating system in supplemented Ham's F12 media were placed directly on top of cells in each well at a final volume of 0.2 mL and incubated at 37°C and 5% CO_2 for two hours. The incubation time was selected to represent the pharmacologic half-life of CP but is a compromise between the wide range of reported half-lives for each species. After the incubation period, cells were washed once with Hanks Balanced Salt Solution (Corning 21-021-CV, Corning, NY) and then supplemented Ham's F12 media was refreshed in each well. Nuclear fluorescence was monitored every three hours by IncuCyte®. After 72 hours post-wash, cell number was compiled over time as "red cell count / mm^2" and normalized to the initial cell count. Fraction of control growth, labeled as "Cell Survival", was then calculated as the measure of cytotoxicity. Cytotoxicity assays were performed in biological triplicate, with each replicate in technical triplicate, for each microsome source used.

Kinetic Modeling of 4OHCP Exposure

The formation of 4OHCP and loss of CP were simulated *in silico* using MATLAB. Equations to describe 4OHCP formation (Michaelis-Menten equation) and CP loss (negative Michaelis-Menten equation) over time were designed as a system of ordinary differential equations (ODEs) and, when solved, represent a numerical solution to integrating the Michaelis-Menten equation. The empirically estimated kinetic parameters (K_M, V_{max}), microsomal protein concentration, and reaction volume were used as constants. A chosen initial CP concentration and a concentration of 0 μM 4OHCP were used as initial conditions. The system of ODEs was solved throughout a specified time frame using the MATLAB "ode45" solver. The output of the kinetic simulation is molar quantities of CP and 4OHCP. The accuracy of the simulation to model kinetic behavior was tested by simulating the discontinuous kinetics assays, described earlier in the Methods, and re-estimating the kinetics parameters (Supplemental Table 1). This model assumes max kinetic efficiency and ignores off-target metabolism.

Cytotoxicity assays were simulated using the above described model with each microsome used *in vitro* (H1, D4, C2, and M3). Concentration of 4OHCP vs. time for each cytotoxicity assay was calculated by simulating reaction conditions, and exposure was calculated as the area under the curve (AUC) of predicted [4OHCP] vs. time using the trapezoidal method, and then correlated to cell survival/fraction of control growth. We chose to use AUC because it captures more information about the time-dependent exposure to 4OHCP, an intermediate in the CP biotransformation pathway (Figure 1), than a single timepoint concentration.

PK Study in Mice

Mouse model protocols were approved by the Institutional Animal Care and Use Committee at Colorado State University. Female NIH CD-1 Swiss mice, 21 total mice at 3 mice per time point, were treated with 100 mg/kg IV cyclophosphamide prepared in 0.9% veterinary grade saline. Whole blood was harvested throughout a time range of 0.08 to 4 hours and was transferred to tubes containing sodium heparin. Blood was spun at 1200x*g* for 10 minutes at 4°C. 100 µL plasma was subsequently transferred to a separate tube containing 10 µL 2M SCZ, vortex mixed, and frozen at -80°C. Plasma CP and 4OHCP were quantified via LC-MS/MS.

Western Blots and Densitometry Calculations

Microsomal CYP2B protein expression was visualized by western blot. Microsomes were prepared in loading buffer (32.9 mM Tris-HCl pH 6.8, 13.2% glycerol, 1.1% SDS, and 0.005% bromophenol blue) and boiled at 95°C for 5 minutes. 15 µg of microsomal protein from each species was loaded per well and proteins were separated via SDS-PAGE using an 8-16% Tris-HCl Mini-PROTEAN TGX stain-free precast gel (Bio-Rad Laboratories, Hercules CA). Proteins were transferred to a PVDF membrane using the Trans-Blot® Turbo™ transfer system (Bio-Rad Laboratories). Transfer was accomplished at 1.3A for 7 minutes. The membrane was blocked in 5% skim milk prepared in tris-buffered saline + 0.2% Tween 20 (TBS-T) for 1 hour at room temperature, incubated with primary antibody (diluted 1:1000) overnight in 5% milk at 4°C,

DMD Fast Forward. Published on December 19, 2018 as DOI: 10.1124/dmd.118.083766
This article has not been copyedited and formatted. The final version may differ from this version.

washed three times with TBS-T, and incubated with secondary antibody (0031430, 1:10000, ThermoFisher Scientific, IL) in 1% milk for 2 hours at room temperature. The antibody used to probe for CYP2B (MA5-25882, clone OTI3D5, ThermoFisher Scientific, IL) is a monoclonal antibody targeting human CYP2B6 and has known cross-species reactivity against dog and mice. Cross-species reactivity against cats is unpublished but anticipated considering sequence homology between the orthologs (Supplemental Table 3). Blots were developed by chemiluminesence using the Clarity™ Western ECL substrate (Bio-Rad Laboratories) and total protein was determined using the stain-free feature of the Bio-Rad ChemiDoc MP system. Relative density of detected protein was calculated by dividing the pixel intensity of the chemiluminescent protein band by the pixel intensity of total lane protein using Fiji software (Schindelin et al., 2012, Schneider et al., 2012). Three independent western blots were developed and an average relative density and standard deviation was then calculated for each microsome source.

Semi-physiologic Modeling of CP Pharmacokinetics

To investigate the accuracy of microsomal metabolism of CP for each species *in vivo,* the observed K_M and V_{max} values were applied to a semi-physiological pharmacokinetic model. The model consisted of three flow-limited compartments representative of whole blood, liver, and the remainder of the body (Figure 5). Physiologic tissue mass and blood flow were applied for each species as described for mouse, dog, and human (Brown et al., 1997), and for cat (unpublished data, allometric scaling) as presented in Table 3. To fully capture the effect of metabolism on CP PK, the model was simplistically designed. Assumptions include: IV dosing (bolus or infusion depending on clinical data used); equal tissue:plasma partitioning; clearance only in the hepatic space based on observed K_M, V_{max}, and cited microsomal protein per gram of liver (P_{mic}) for each species as presented in Table 3. Protein binding was incorporated in the human model at roughly 50% fraction unbound (Bagley et al., 1973), where CP exhibits a low extraction ratio in the liver. In non-human species CP exhibits a high extraction ratio in the liver

and so the models were insensitive to changes in protein binding. For non-human species protein binding was not included, which is physiologically-representative of drug dissociation within the hepatic space for high extraction drugs (Meijer and van der Sluijs, 1989). Parameters included in the model were used as the cited value in literature and were not optimized for the simulation. Simulation output was compared against clinically-obtained CP PK data for each species at the appropriate dose.

Scaling of the microsomal V_{max} to represent liver V_{max} *in vivo* was described by Equation 1. Equations for the rest of the body, liver, and plasma were represented by equations 2, 3, and 4, respectively:

$$V_{max}^{liv} = V_{max}^{mic} \cdot P_{mic} \cdot V_{liv} \quad (1)$$

$$\frac{dm_{rb}}{dt} = Q_{rb} \cdot (C_a - C_{v,rb}) \quad (2)$$

$$\frac{dm_{liv}}{dt} = Q_{liv} \cdot (C_a - C_{v,liv}) - \left(\frac{C_{liv} \cdot V_{max}^{liv}}{K_m \cdot C_{liv}}\right) \quad (3)$$

$$\frac{dm_{pl}}{dt} = Q_{liv} \cdot (C_{v,liv} - C_a) - Q_{rb} \cdot (C_{v,rb} - C_a) \quad (4)$$

Where m_x is the amount of CP within the compartment, C_a is the arterial plasma concentration of CP, $C_{v,x}$ is the venous plasma concentration of CP leaving each tissue where *x* can represent *liv* (liver) or *rb* (rest of body), P_{mic} is the microsomal protein per gram of liver, C_{liv} is the total concentration of CP in the liver, V_{liv} is the volume of the liver, Q_x is the blood flow rate to each tissue, and K_m and V_{max} are Michaelis-Menten rate constants obtained in this study.

Computer Simulation and Software

The kinetics simulation model and semi-physiologic pharmacokinetic model were implemented in MATLAB version R2018a from The MathWorks, Inc. (Natick, MA). Clinical and

simulated pharmacokinetic metrics were calculated via noncompartmental analysis on Phoenix 64 WinNonlin build 8.0.0.3176, Certara LP (St. Louis, MO).

RESULTS

Species-Dependent Differential Kinetics of 4OHCP Formation in Microsomes

Microsomes from humans, dogs, cats, and mice were used to determine the kinetics of 4OHCP formation (Figure 2). Microsome source information, including species identification used throughout the rest of the manuscript (H = human, D = dog, C = cat, M = mouse) is included in Table 1. 4OHCP formation was determined to be linear at the times described in the methods, satisfying the steady-state assumption (data not shown). Curves were fit and kinetic parameters were estimated under the assumption of a Michaelis-Menten one-enzyme model (Table 2). Curves for microsomes D1 and C2 were performed at CP concentrations dissimilar to the other microsomes because they were the first to be tested, and we had no remaining microsomes from these sources to redo the assays at the ranges shown for the rest of the microsomes. There were no data points left out of any curve for the kinetics analysis (see Methods). Comparison of V_{max}/K_M, presented here as intrinsic clearance (CL_{int}), suggests a metabolic stratification between the different species. Dog microsomes were, on average, 55-fold more efficient than human microsomes, 2.8-fold more efficient than cat microsomes, and 1.2-fold more efficient than mouse microsomes at catalyzing CP bioactivation.

The assumption of the one-enzyme model was evaluated by transforming the Michaelis-Menten plots in Figure 2 according to the Eadie-Hofstee linearization (Supplemental Figure 1). For all Eadie-Hofstee data, we compared the fit of a line versus exponential decay and selected the best of the two using Akaike Information Criterion corrected for small sample size (AICc) implemented in GraphPad Prism 7.0d (La Jolla, CA). Despite no evidence of atypical kinetic behavior in the Michaelis-Menten plots, linearization and subsequent fit comparisons revealed that M1, M2, and M3 kinetics behave in a biphasic fashion (Supplemental Figure 1A). Kinetics data for microsome C1 visually can resemble either an exponential decay or a line; indeed, model comparison selected exponential decay to describe C1 but with remarkably less confidence compared to the model selections for M1, M2, or M3 (data not shown). Thus, C1

kinetic behavior was regarded as monophasic in agreeance with the assumptions made above. The biphasic behavior for M1, M2, and M3 was separated into a “fast” and “slow” set of kinetic parameters, defined as low-affinity/high-turnover and high-affinity/low-turnover, respectively. These parameters are presented in Supplemental Figure 1B. Notably, the fast kinetic parameters for each microsome are similar the monophasic parameters estimated from nonlinear regression.

We designed a kinetic simulation model in MATLAB that simulates concentration versus time curves for the metabolic conversion of CP to 4OHCP, as described in the Methods. This model was tested using each set of microsomal kinetic parameters by simulating the discontinuous kinetics assay and re-estimating the kinetics parameters to verify accuracy of the simulation model as shown in Supplemental Figure 2. Supplemental Table 1 contains the comparison of empirical to simulated kinetics parameters for each microsomal source. In all cases the simulation model over predicts the kinetics parameters, but on average by no more than 2.4% of empirical. This demonstrates that the observed microsomal kinetics can be adequately modeled by monophasic kinetics within reasonable error.

Microsomal Kinetics Predict *in vitro* Cell Death

We sought to further investigate the *in vitro* differential 4OHCP formation kinetics as a precursor to evaluating clinical data. As a first measure of understanding *in vitro* metabolic differences, the conversion of CP to 4OHCP was monitored using the XenoTech-derived microsomes in 0.1 M phosphate buffer. Using a constant CP concentration (7.6 μM), time point (30 minutes), and protein concentration (0.5 mg/mL) for each microsome (H1, D4, C2, M3), the percentage of CP metabolized into 4OHCP was determined to be 2.59% for H1, 39.23% for D4, 19.06% for C1, and 23.23% for M3 from one experiment. Additionally, theoretical 4OHCP formation was estimated from the loss of CP under the assumption of 100% conversion to measurable 4OHCP (from the same experiment above); for each microsome the ratio of

measurable to theoretical 4OHCP is 0.3408 for H1, 0.7846 for D4, 0.8311 for C2, and 0.8630 for M3. These data demonstrate that the primary metabolite formed *in vitro* is 4OHCP for only the nonhuman microsomes. Furthermore, this implies that *in vitro* manifestations of metabolic differences should also be apparent in cellular-based systems.

To that end, we designed a cytotoxicity assay that mimics 4OHCP drug exposure to MDA-MB-231 human breast cancer cells, selected because triple negative breast cancers, from which MDA-MB-231 is derived, are commonly treated with cyclophosphamide and thus is a clinically representative *in vitro* model to study CP cytotoxicity. We first determined the effect of Ham's F12 media – which is used for maintaining MDA-MB-231 cells – on microsome catalytic activity by re-estimating the kinetic parameters in microsomes from Sekisui XenoTech, LLC (Kansas City, KS) (H1, D4, C2, and M3). These were selected due to microsome quantity constraints. The kinetic parameters for each XenoTech microsome source in Ham's F12 media is as follows [V_{max} ± *S.E. (pmol 4-OHCP/min/mg-protein),* K_M ± *S.E. (μM)]*: H1 [3793 ± 325.1, 1885 ± 553.4], D4 [4733 ± 381.3, 83.10 ± 15.47], C2 [752.8 ± 40.64, 50.98 ± 7.413], and M3 [9425 ± 461.5, 93.02 ± 10.15]. The V_{max} estimated in Ham's F12 media increased relative to parameters estimated in 0.1 M phosphate buffer, and the K_M decreased for all but C2. Intrinsic clearances (V_{max}/K_M) compared between the two media conditions are shown in Supplemental Table 2 and demonstrate that H1, D4, and M3 microsomes become more catalytically active in Ham's F12 media relative to phosphate buffer. The calculated intrinsic clearance of C2 microsomes in Ham's F12 relative to phosphate buffer decreased by 0.7590-fold. The kinetic profiles from Ham's F12 media were Eadie-Hofstee transformed, following the workflow described in the methods, and none of the kinetics displayed biphasic kinetics (data not shown). This contrasts the behavior observed for M3 in phosphate buffer.

For the cytotoxicity assay, we treated cells with microsomes and CP at a range from 3.8 – 3831 μM for two hours, then monitored cytotoxicity and quantified cell death after 72 hours via IncuCyte® imaging. These concentrations were chosen to encompass a wide range of

pharmacologic CP concentrations observed at clinically relevant doses, which includes: cat C_{max} = 35.2 μM (Stroda et al., 2017), dog C_{max} = 78.5 μM (Warry et al., 2011), mouse C_{max} = 204.1 μM, and human C_{max} = 700 μM (Chen et al., 1995). Non-pharmacologic concentrations of CP were also included to fully capture cytotoxic phenomena. We observed cytotoxicity profiles that resemble traditional dose-response curves (Figure 3A). Cell survival was normalized as fraction of control for each microsome condition so that comparisons could be made across each species. Cells treated either with dog or mouse microsomes demonstrated the greatest response relative to cat microsomes, which produced an intermediate sensitivity phenotype, and human microsomes, which demonstrated the least sensitivity. The IC_{50} estimates for each curve are as follows: H1, 1857 μM; D4, 31.65 μM; C2, 272.6 μM; and M3, 44.95 μM.

The cytotoxicity curves only consider the initial CP concentration as it relates to cell death; exposure of 4OHCP is the more important measure as 4OHCP directly transforms to the cytotoxic agent, PM. To understand the relationship between 4OHCP exposure and cell death, we used the kinetic simulation model described previously in the text. 4OHCP concentration was simulated for each cytotoxicity experiment using this simulation model and the resultant exposure was predicted and related to cell death (Figure 3B). Correlations between cell death and predicted 4OHCP exposure were calculated for human (Spearman ρ = -0.6, P = 0.0968), dog (Spearman ρ = -1; ***P < 0.001), cat (Spearman ρ = -0.9333, ***P < 0.001), and mouse (Spearman ρ = -0.9643, **P < 0.01) microsomes. The Spearman correlation between overall cell death and predicted exposure, without separating the data by species, was significant (Spearman ρ = -0.8691; 95% CI: -0.9359, -0.7420; ****P < 0.0001). This model makes two assumptions: (1) 100% of produced 4OHCP is converted to PM and available for alkylation; and (2) activation of off-target metabolic pathways throughout the assay is negligible.

Since CYP2B6 is hypothesized to be the critical metabolizing enzyme for CP bioactivation (see Introduction), we sought to characterize the *in vitro* expression *of* CYP2B orthologs in these microsomes. We compared orthologous CYP2B sequences between the four

studied species, based on published canonical sequences, and found a high degree of homology between each sequence (Supplemental Table 3). The lowest percentage of homology was observed between cat and mouse orthologs at 84.2%, whereas the highest percentage of homology was observed between cat and dog orthologs at 91%.

The CYP2B expression status for available microsomes was determined via western blot (Figure 4A), and consistent protein loading was confirmed by total protein scan (Supplemental Figure 3). Densitometry was employed to determine the relative density of each chemilumiescent CYP2B protein band against the total protein (Supplemental Table 4). Mouse microsomes expressed the most CYP2B: 3.1-fold more than dogs, 7.5-fold more than humans, and 203-fold more than cats, on average. The virtually undetectable CYP2B ortholog in C2 cat microsomes is notable. Means (without standard deviation) of densitometry calculations from three independent western blots probing CYP2B (Supplemental Table 4) were plotted (along the abscissa) against microsomal V_{max}; there exists a statistically significant Spearman correlation between these two variables (Spearman $\rho = 0.8333$; $^{*}P < 0.05$) (Figure 4B).

In addition to CYP2B, we sought to understand the contribution of CYP2C9/2C19 and CYP3A4 orthologs in CP bioactivation for each of the species. Antibodies targeting these orthologs are not readily available for cross-reactivity against our species panel, so we used chemical inhibitors to ablate CYP activity in each of the XenoTech (H1, D4, C2, and M3) microsomes and observed the effect on CP bioactivation. Microsomal 4OHCP formation was measured in the presence of each CYP inhibitor (Figure 4C). 4OHCP formation is presented as the AUC from the 4OHCP concentration vs. time curve for each condition normalized to the CP control condition (see Methods). Ketoconazole, inhibitor of CYP3A4, has no apparent impact on 4OHCP formation in any of the microsomes. This is similarly true for miconazole, inhibitor of CYP2C19 and CYP3A4, though a slight enzyme impedance is observed in the dog and human microsomes. CBP, inhibitor of CYP2B6, has relatively little influence on 4OHCP formation except in cat microsomes, where it significantly reduces enzyme activity (ratio of $AUC_{+CP,CBP}$ /

AUC_{+CP} = 0.227). Fluconazole, inhibitor of CYP2C9 and CYP3A4, inhibits 4OHCP formation the greatest and affects all four species tested. Most notable is the effect of fluconazole in dog microsomes which results in near complete ablation of 4OHCP formation (ratio of $AUC_{+CP,Fluconazole}$ / AUC_{+CP} = 0.0148). Two additional inhibitors specific to canine CYPs were tested in dog microsomes only. Sulfaphenazole, inhibitor of canine CYP2C21/41, reduces 4OHCP formation by nearly half compared to control, and chloramphenicol, inhibitor of CYP2B11, does not inhibit 4OHCP formation.

Microsomal 4OHCP Formation Kinetics Influences CP Pharmacokinetics

To further understand the influence of *in* vitro metabolism on CP PK and assess the *in vivo* accuracy of the observed 4OHCP formation kinetics, microsomal kinetics parameters were incorporated into a 3-compartment semi-physiological PK model and compared against clinically-obtained PK data. PK data from mice were generated following a single IV dose of CP at 100 mg/kg. Whole blood and organs were harvested at 0.08, 0.25, 0.5, 1.0, 2.0, 3.0, and 4.0 hours after dosing. CP concentrations in plasma were used (Supplemental Figure 4). Plasma PK data from canine (Warry et al., 2011), feline (Stroda et al., 2017), and human (Struck et al., 1987, Chen et al., 1995) patients were also used in the model. Simulated PK data from the model were compared against the IV dosing scheme (bolus or infusion) and clinical PK data. The model closely simulated the mean plasma CP concentrations of each animal species as depicted in Figure 6 (animal graphs), and two human studies in Figure 7 (human graphs).

The ability of the model to accurately predict CP PK was determined by comparing parameters derived from noncompartmental analysis (Table 4). Area under the curve (AUC) and half-life ($t_{1/2}$) for clinical and simulated data were compared ratiometrically. Dog, cat, and mouse comparisons result in respective AUC simulated/actual ratios of 1.07, 1.39, 2.35, and $t_{1/2}$ of 1.09, 1.38, 1.21 (Figure 6). Model output using each species' scaled kinetic parameters incorporated into the semi-physiologic model was remarkably similar between each batch of microsomes,

emphasizing the blood flow-limited nature of CP metabolism in these species. For both human PK studies, the model tended to underestimate the AUC, with simulated/actual ratios of 0.79 and 0.58, and slightly overestimate the half-life, with simulated/actual ratios of 1.15 and 1.60. In both PK studies, H3 exhibited the best performance when applied to the semi-physiological model.

DISCUSSION

The need for better understanding of animal CP metabolism, within the context of veterinary research, warranted the current study. The data herein demonstrates the importance of *in vitro* metabolism on CP PK in species frequently treated with CP and the utility of post-hoc clinical modeling in coordination with pre-clinical data to understand important factors of pharmacokinetics. Physiologically-based pharmacokinetic (PBPK) modelling largely serves this purpose, but the present study highlights the common paradigm in mathematical modeling that simple models can produce fruitful interpretations (Gunawardena, 2014).

The present study is not the first to investigate CP metabolism in humans; the kinetic parameters presented herein are similar to published data derived from liver metabolic data (Anderson et al., 1996), microsomes (Ren et al., 1997), and supersomes (Roy et al., 1999, Huang et al., 2000). Likewise, the presented dog parameters are comparable to other published studies (Chen et al., 2004, Lautier et al., 2016). Parameters for cat and mouse microsomes, in contrast, have not been published. The presentation of biphasic 4OHCP formation kinetics from microsomal systems (i.e. in the studied mouse sources), while interesting, is not sufficient to demonstrate the nature of the kinetic mechanisms at play. Certain CYP enzymes are known to behave in ways that are not in full agreeance with Michaelis-Menten kinetics, but when experiments are performed using multi-enzyme systems - such as with liver microsomes - observed atypical kinetics may be artifactual instead of real (Hutzler and Tracy, 2002). For example, previous characterization of human liver microsomes were decidedly biphasic in regards to 4OHCP formation kinetics (Ren et al., 1997), yet data in the current study contradicts that finding. It is unknown how much either of these data were influenced by artifactual biases. It is important to remember that CYPs involved in xenobiotic metabolism are generally considered catalytically promiscuous because these enzymes can display broad specificity for substrates (Bernhardt, 2006). Thus, observing biphasic kinetics from microsomes might not be surprising considering what is currently known about CYP contributions to CP metabolism. Nevertheless,

apparent monophasic kinetics obtained from microsomes are still useful and are important for many aspects of drug discovery (Vrbanac and Slauter, 2013). Indeed, when comparing kinetic parameters and particularly the microsomal intrinsic clearance among sources H1, D4, C2, and M3, the monophasic kinetics predict the differences in observed cytotoxicity profiles and calculated IC_{50} values. We did not observe a significant correlation between cell survival and predicted 4OHCP exposure in human microsomes in contrast to the others, but we attribute this to the undetectable cell death at the majority of CP concentrations tested and would expect to see a correlation if we extended the CP range well beyond the already non-pharmacologically relevant concentrations.

The importance of human CYP2B6 in CP metabolism has been studied extensively, and although several isozymes are believed to contribute to CP hydroxylation, CYP2B6 is frequently singled-out as most significant (Xie et al., 2003, Rodriguez-Antona and Ingelman-Sundberg, 2006). The undetectable CYP2B ortholog in short-hair cats is unexpected, but a recent study has demonstrated that cats lack apparent liver expression of their CYP2B ortholog (Okamatsu et al., 2017). Some human liver microsomes derived from patients evidently lack CYP2B6 expression, but not to the same extent as cats (Xie et al., 2003). Importantly, humans are not known to express CYP2B6 anywhere but the liver (Thelen and Dressman, 2009). As for canines, beagles have been shown to express CYP2B11, their CYP2B6 ortholog (Heikkinen et al., 2012), but differential expression across breeds is undocumented, and its effect on overall CP metabolism has remained elusive. While increasing age (≥adult) has been thought to influence CYP expression, studies suggest that in humans and dogs only CYP activity seems to be negatively impacted (Tibbitts, 2003, Zanger and Schwab, 2013).

As mentioned previously, several CYPs have been implicated in the bioactivation of CP. The data presented herein demonstrates that ketoconazole failed to inhibit 4OHCP formation suggesting that CYP3A4 and its animal orthologs contribute very little to the formation of 4OHCP. Fluconazole, the CYP2C9 inhibitor, had the greatest impact on 4OHCP formation in

humans compared to the CYP2B6 (CBP) and CYP2C19 (miconazole) inhibitor, though we conclude that both CYP2C9 and CYP2B6 are involved CP metabolism. This conclusion is shared with mice, assuming fluconazole and CBP inhibit mouse CYP2C and CYP2B, respectively. Cats were the only species appreciably sensitive to CBP - the CYP2B6 inhibitor - but considering the lack of CYP2B detected in the western blot, it seems likely that CBP has a different CYP isozyme target in cats than the other species. No tested inhibitor completely ablated CP metabolism activity in humans, cats, or mice. In contrast, dog microsomal metabolism of 4OHCP is almost completely inhibited by fluconazole. Treatment with the canine CYP2C-specific inhibitor sulfaphenzole only slightly recapitulated the phenomenon observed with fluconazole. There was no observed impact of 4OHCP production when dog microsomes were treated with CYP2B inhibitors. The results propose the conclusion that CYP2C seems to be more significant than CYP2B in the metabolism of CP to 4OHCP.

This is at odds with what has been published previously. The results from a recent study identified three important CYP active site residues that contribute to CP binding and recognition and that the dog ortholog (CYP2B11) contains mutations in these residue locations that renders it one of the most efficient enzymes at catalyzing CP hydroxylation (Chen et al., 2004). Rational engineering studies of CYP2B6 identified a residue substitution, L264F, that confers greater stability and metabolic activity to human CYP2B6 (Kumar et al., 2007). This phenylalanine residue is also found within the dog, cat, and mouse CYP2B protein sequences. Moreover, as a test of CYP2B and its role in CP bioactivation, gliosarcoma cells stably transfected with rat CYP2B1 became significantly more sensitive to 4OHCP and were capable of catalyzing CP bioactivation (Chen and Waxman, 1995). All these data tell a story that the CYP2B isozyme is significant for 4OHCP formation. The data presented in Figure 4B, demonstrating a significant correlation between V_{max} and relative CYP2B expression, suggests the same. It is important to note that the mathematical expression for $V_{max} = k_{cat}*[enzyme]_{total}$ contains a species dependent apparent rate constant (k_{cat}) that for a multienzyme system represents the contribution of each

enzyme involved. A direct comparison between V_{max} and CYP2B expression is thus inappropriate, but a generalized interpretation would suggest not only that the apparent k_{cat} for CP transformation follows a trend among the species, but also that it appears to be influenced by CYP2B expression. Thus, considering published data, we favor a conclusion that CYP2C is a critical factor alongside CYP2B in determining CP bioactivation, particularly in canines.

Incorporating microsomal-derived Michaelis-Menten parameters into a semi-physiological pharmacokinetic model using metabolism as the only form of clearance indicates the significance of CP metabolism in its overall PK profile. For the three animal species examined (dog, cat, and mouse), the simulation predicted comparable half-lives and AUCs to clinical data between microsomal sources. This observation supports the clinical applicability of microsome-obtained metabolism parameters for these species but emphasizes the importance of small changes in blood flow to the liver rather than metabolic parameters as the driver of PK variability. In humans, the model generally underestimated overall CP exposure and slightly overestimated the half-life. Unlike dog, cat, and mouse microsomes, different batches of human microsomes exhibited remarkably different simulated PK when incorporated into the model. This is due to the significantly lower rate of metabolism in humans which causes CP to behave as a low liver extraction drug, rather than high as observed in the non-human species. For this reason, small changes in metabolic parameters will significantly influence human CP PK *in vivo*, whereas non-human species are more significantly influenced by blood flow to the liver. Based on the two human CP PK studies used for comparison, H3 exhibited the most representative metabolic parameters of the patient population and parameters obtained from this source could be scaled accurately for *in vivo* simulation.

The human simulations compared to clinical PK indicates the potential application of microsomes to predict metabolism yet emphasizes the variability that may be observed *in vivo* due to alterations in metabolic parameters. The simulated human half-lives, though slightly overestimated compared to the two studies, still fit within the range of observed CP half-lives

when compared to scores of PK studies (3.2 - 12.5 hours) (de Jonge et al., 2005), albeit near the lower end of that range.

These conclusions present an important view of differential CP metabolism in animals and humans, and provide new insight to support the significance of multiple CYP isozymes in the hepatic bioactivation and clearance of CP. This study also demonstrates the utility of *in vitro* metabolic characterization and that such data is crucial to understanding CP PK in humans, dogs, cats, and mice.

AUTHORSHIP CONTRIBUTIONS

Participated in research design: Ramirez and Gustafson.

Conducted experiments: Ramirez, Conger, and Aradi.

Contributed new reagents or analytic tools: Ramirez and Collins.

Performed data analysis: Ramirez and Collins.

Wrote or contributed to the writing of the manuscript: Ramirez, Collins, Aradi, and Gustafson.

REFERENCES

Ahmed AR and Hombal SM (1984) Cyclophosphamide (Cytoxan). A review on relevant pharmacology and clinical uses. *J Am Acad Dermatol* **11:** 1115-1126.

Anderson LW, Chen TL, Colvin OM, Grochow LB, Collins JM, Kennedy MJ and Strong JM (1996) Cyclophosphamide and 4-hydroxycyclophosphamide/aldophosphamide kinetics in patients receiving high-dose cyclophosphamide chemotherapy. *Clin Cancer Res* **2:** 1481-1487.

Back DJ, Tjia JF, Karbwang J and Colbert J (1988) In vitro inhibition studies of tolbutamide hydroxylase activity of human liver microsomes by azoles, sulphonamides and quinolines. *Br J Clin Pharmacol* **26:** 23-29.

Bagley CM, Jr., Bostick FW and DeVita VT, Jr. (1973) Clinical pharmacology of cyclophosphamide. *Cancer Res* **33:** 226-233.

Barter ZE, Bayliss MK, Beaune PH, Boobis AR, Carlile DJ, Edwards RJ, Houston JB, Lake BG, Lipscomb JC, Pelkonen OR, Tucker GT and Rostami-Hodjegan A (2007) Scaling Factors for the Extrapolation of In Vivo Metabolic Drug Clearance From In Vitro Data: Reaching a Consensus on Values of Human Microsomal Protein and Hepatocellularity Per Gram of Liver. *Curr Drug Metab* **8:** 33-45.

Bernhardt R (2006) Cytochromes P450 as versatile biocatalysts. *J Biotechnol* **124:** 128-145.

Boddy AV and Yule SM (2000) Metabolism and pharmacokinetics of oxazaphosphorines. *Clin Pharmacokinet* **38:** 291-304.

Brown RP, Delp MD, Lindstedt SL, Rhomberg LR and Beliles RP (1997) Physiological parameter values for physiologicall based pharmacokinetic models. *Toxicol Ind Health* **13:** 407-484.

Carlile DJ, Hakooz N, Bayliss MK and Houston JB (2001) Microsomal prediction of in vivo clearance of CYP2C9 substrates in humans. *Br J Clin Pharmacol* **47:** 625-635.

Chen CS, Lin JT, Goss KA, He YA, Halpert JR and Waxman DJ (2004) Activation of the anticancer prodrugs cyclophosphamide and ifosfamide: identification of cytochrome P450 2B enzymes and site-specific mutants with improved enzyme kinetics. *Mol Pharmacol* **65:** 1278-1285.

Chen L and Waxman DJ (1995) Intratumoral activation and enhanced chemotherapeutic effect of oxazaphosphorines following cytochrome P-450 gene transfer: development of a combined chemotherapy/cancer gene therapy strategy. *Cancer Res* **55:** 581-589.

Chen T, Passos-Coelho J, Noe D, Kennedy M, Black K, Colvin O and Grochow L (1995) Nonlinear pharmacokinetics of cyclophosphamide in patients with metastatic breast cancer receiving high-dose chemotherapy followed by autologous bone marrow transplantation. *Cancer Research* **55:** 810-816.

de Jonge ME, Huitema AD, Rodenhuis S and Beijnen JH (2005) Clinical pharmacokinetics of cyclophosphamide. *Clin Pharmacokinet* **44:** 1135-1164.

Eagling VA, Tjia JF and Back DJ (1998) Differential selectivity of cytochrome P450 inhibitors against probe substrates in human and rat liver microsomes. *Br J Clin Pharmacol* **45:** 107-114.

Emadi A, Jones RJ and Brodsky RA (2009) Cyclophosphamide and cancer: golden anniversary. *Nat Rev Clin Oncol* **6:** 638-647.

Garrett LD, Thamm DH, Chun R, Dudley R and Vail DM (2002) Evaluation of a 6-month chemotherapy protocol with no maintenance therapy for dogs with lymphoma. *J Vet Intern Med* **16:** 704-709.

Gibhard L, Pravin K, Abay E, Wilhelm A, Swart K, Lawrence N, Khoury R, Westhuizen Jvd, Smith P and Wiesnera L (2016) In Vitro and In Vivo Pharmacokinetics of Aminoalkylated Diarylpropanes NP085 and NP102. *Antimicrob Agents Chemother* **60:** 3065-3069.

Groehler At, Villalta PW, Campbell C and Tretyakova N (2016) Covalent DNA-Protein Cross-Linking by Phosphoramide Mustard and Nornitrogen Mustard in Human Cells. *Chem Res Toxicol* **29:** 190-202.

Gunawardena J (2014) Models in biology: 'accurate descriptions of our pathetic thinking'. *BMC Biol* **12:** 29.

Heikkinen AT, Friedlein A, Lamerz J, Jakob P, Cutler P, Fowler S, Williamson T, Tolando R, Lave T and Parrott N (2012) Mass spectrometry-based quantification of CYP enzymes to establish in vitro/in vivo scaling factors for intestinal and hepatic metabolism in beagle dog. *Pharm Res* **29:** 1832-1842.

Huang Z, Roy P and Waxman DJ (2000) Role of human liver microsomal CYP3A4 and CYP2B6 in catalyzing N-dechloroethylation of cyclophosphamide and ifosfamide. *Biochem Pharmacol* **59:** 961-972.

Huitema A, Tibben M, Kerbusch T, Kettenes-van den Bosch J, Rodenhuis R and Beijnen JH (2000) High performance liquid-chromatographic determination of the stabilized cyclophosphamide metabolite 4-hydroxycyclophosphamide in plasma and red blood cells. *J Liq Chromatogr Rel Technol* **23:** 1725-1744.

Hutzler JM and Tracy TS (2002) Atypical kinetic profiles in drug metabolism reactions. *Drug Metab Dispos* **30:** 355-362.

Jia L and Liu X (2007) The conduct of drug metabolism studies considered good practice (II): in vitro experiments. *Curr Drug Metab* **8:** 822-829.

Korhonen LE, Turpeinen M, Rahnasto M, Wittekindt C, Poso A, Pelkonen O, Raunio H and Juvonen RO (2007) New potent and selective cytochrome P450 2B6 (CYP2B6) inhibitors based on three-dimensional quantitative structure-activity relationship (3D-QSAR) analysis. *Br J Pharmacol* **150:** 932-942.

Kumar S, Zhao Y, Sun L, Negi SS, Halpert JR and Muralidhara BK (2007) Rational engineering of human cytochrome P450 2B6 for enhanced expression and stability: importance of a Leu264->Phe substitution. *Mol Pharmacol* **72:** 1191-1199.

Kunze KL, Wienkers LC, Thummel KE and Trager WF (1996) Warfarin-fluconazole. I. Inhibition of the human cytochrome P450-dependent metabolism of warfarin by fluconazole: in vitro studies. *Drug Metab Dispos* **24:** 414-421.

Kuroha M, Kuze Y, Shimoda M and Kokue E (2002) In vitro characterization of the inhibitory effects of ketoconazole on metabolic activities of cytochrome P-450 in canine hepatic microsomes. *Am J Vet Res* **63:** 900-905.

Lautier T, Urban P, Loeper J, Jezequel L, Pompon D and Truan G (2016) Ordered chimerogenesis applied to CYP2B P450 enzymes. *Biochim Biophys Acta* **1860:** 1395-1403.

Li F, Patterson AD, Hofer CC, Krausz KW, Gonzalez FJ and Idle JR (2010) Comparative metabolism of cyclophosphamide and ifosfamide in the mouse using UPLC-ESI-QTOFMS-based metabolomics. *Biochem Pharmacol* **80:** 1063-1074.

Meijer DKF and van der Sluijs P (1989) Covalent and Noncovalent Protein Binding of Drugs: Implications for Hepatic Clearance, Storage, and Cell-Specific Drug Delivery. *Pharm Res* **6:** 105-118.

Miners JO and Birkett DJ (1998) Cytochrome P4502C9: an enzyme of major importance in human drug metabolism. *Br J Clin Pharmacol* **45:** 525-538.

Moghe A, Ghare S, Lamoreau B, Mohammad M, Barve S, McClain C and Joshi-Barve S (2015) Molecular mechanisms of acrolein toxicity: relevance to human disease. *Toxicol Sci* **143:** 242-255.

Niwa T, Shiraga T and Takagi A (2005) Effect of antifungal drugs on cytochrome P450 (CYP) 2C9, CYP2C19, and CYP3A4 activities in human liver microsomes. *Biol Pharm Bull* **28:** 1805-1808.

Okamatsu G, Komatsu T, Ono Y, Inoue H, Uchide T, Onaga T, Endoh D, Kitazawa T, Hiraga T, Uno Y and Teraoka H (2017) Characterization of feline cytochrome P450 2B6. *Xenobiotica* **47:** 93-102.

Pearce RE, McIntyre CJ, Madan A, Sanzgiri U, Draper AJ, Bullock PL, Cook DC, Burton LA, Latham J, Nevins C and Parkinson A (1996) Effects of freezing, thawing, and storing human liver microsomes on cytochrome P450 activity. *Arch Biochem Biophys* **331:** 145-169.

Penel N, Adenis A and Bocci G (2012) Cyclophosphamide-based metronomic chemotherapy: after 10 years of experience, where do we stand and where are we going? *Crit Rev Oncol Hematol* **82:** 40-50.

Perez Jimenez TE, Mealey KL, Schnider D, Grubb TL, Greene SA and Court MH (2018) Identification of canine cytochrome P-450s (CYPs) metabolizing the tramadol (+)-M1 and (+)-M2 metabolites to the tramadol (+)-M5 metabolite in dog liver microsomes. *J Vet Pharmacol Ther*, 10.1111/jvp.12706.

Ren S, Yang J, Kalhorn T and Slattery J (1997) Oxidation of cyclophosphamide to 4-hydroxycyclophosphamide and deschloroethylcyclophosphamide in human liver microsomes. *Cancer Research* **57:** 4229-4235.

Rodriguez-Antona C and Ingelman-Sundberg M (2006) Cytochrome P450 pharmacogenetics and cancer. *Oncogene* **25:** 1679-1691.

Roy P, Yu LJ, Crespi CL and Waxman DJ (1999) Development of a substrate-activity based approach to identify the major human liver P-450 catalysts of cyclophosphamide and ifosfamide activation based on cDNA-expressed activities and liver microsomal P-450 profiles. *Drug Metab Dispos* **27:** 655-666.

Sakaeda T, Iwaki K, Kakumoto M, Nishikawa M, Niwa T, Jin JS, Nakamura T, Nishiguchi K, Okamura N and Okumura K (2005) Effect of micafungin on cytochrome P450 3A4 and

multidrug resistance protein 1 activities, and its comparison with azole antifungal drugs. *J Pharm Pharmacol* **57:** 759-764.

Schindelin J, Arganda-Carreras I, Frise E, Kaynig V, Longair M, Pietzsch T, Preibisch S, Rueden C, Saalfeld S, Schmid B, Tinevez JY, White DJ, Hartenstein V, Eliceiri K, Tomancak P and Cardona A (2012) Fiji: an open-source platform for biological-image analysis. *Nat Methods* **9:** 676-682.

Schneider CA, Rasband WS and Eliceiri KW (2012) NIH Image to ImageJ: 25 years of image analysis. *Nat Methods* **9:** 671-675.

Smith R, Jones R, Ballard P and Griffiths H (2008) Determination of microsome and hepatocyte scaling factors for in vitro/in vivo extrapolation in the rat and dog. *Xenobiotica* **38:** 1386-1398.

Stevenson H and Fauci A (1980) Activation of human B lymphocytes. XII. Differential effects of in vitro cyclophosphamide on human lymphocyte subpopulations involved in B-cell activation. *Immunology* **39:** 391-397.

Stroda KA, Murphy JD, Hansen RJ, Brownlee L, Atencio EA, Gustafson DL and Lana SE (2017) Pharmacokinetics of cyclophosphamide and 4-hydroxycyclophosphamide in cats after oral, intravenous, and intraperitoneal administration of cyclophosphamide. *American Journal of Veterinary Research* **78:** 862-866.

Struck RF, Alberts DS, Horne K, Phillips JG, Peng YM and Roe DJ (1987) Plasma pharmacokinetics of cyclophosphamide and its cytotoxic metabolites after intravenous versus oral administration in a randomized, crossover trial. *Cancer Res* **47:** 2723-2726.

Teske E, van Straten G, van Noort R and Rutteman GR (2002) Chemotherapy with cyclophosphamide, vincristine, and prednisolone (COP) in cats with malignant lymphoma: new results with an old protocol. *J Vet Intern Med* **16:** 179-186.

Thelen K and Dressman JB (2009) Cytochrome P450-mediated metabolism in the human gut wall. *J Pharm Pharmacol* **61:** 541-558.

Tibbitts J (2003) Issues related to the use of canines in toxicologic pathology--issues with pharmacokinetics and metabolism. *Toxicol Pathol* **31 Suppl:** 17-24.

Uphoff C and Drexler H (2013) Detection of Mycoplasma Contaminations, in *Basic Cell Culture Protocols* (Helgason C and Miller C eds) pp 1-14, Totowa, NJ, Humana Press.

Visser M, Zaya M, Locuson C, Booth D and Merritt D (2018) Comparison of predicted intrinsic hepatic clearance of 30 pharmaceuticals in canine and feline liver microsomes. *Xenobiotica*, 10.1080/00498254.2018.1437933.

Vrbanac J and Slauter R (2013) ADME in Drug Discovery, in *A Comprehensive Guide to Toxicology in Preclinical Drug Development* (Faqi AS eds) pp 3-30, Elsevier Inc.

Warry E, Hansen R, Gustafson D and Lana S (2011) Pharmacokinetics of cyclophosphamide after oral and intravenous administration to dogs with lymphoma. *J Vet Intern Med* **25:** 903-908.

Xie HJ, Yasar U, Lundgren S, Griskevicius L, Terelius Y, Hassan M and Rane A (2003) Role of polymorphic human CYP2B6 in cyclophosphamide bioactivation. *Pharmacogenomics J* **3:** 53-61.

Yamazaki H, Inoue K, Turvy CG, Guengerich FP and Shimada T (1997) Effects of freezing, thawing, and storage of human liver samples on the microsomal contents and activities of cytochrome P450 enzymes. *Drug Metab Dispos* **25:** 168-174.

Zanger UM and Schwab M (2013) Cytochrome P450 enzymes in drug metabolism: regulation of gene expression, enzyme activities, and impact of genetic variation. *Pharmacol Ther* **138:** 103-141.

FOOTNOTES

This work was supported by the Shipley University Chair in Comparative Oncology and the Angelo Fund for Feline Therapeutics. Support for animal studies was provided by the University of Colorado Cancer Center Pharmacology Shared Resource [Grant P30CA046934].

FIGURE LEGENDS

Figure 1. Schematic of CP biotransformation.

Figure 2. Michaelis-Menten kinetics of 4OHCP formation in each species of microsome. Kinetics data were collected for (a) human (H), (b) dog (D), (c) cat (C), and (d) mouse (M) microsomes and were fit to a one-enzyme model. Kinetic parameters were estimated in GraphPad Prism v7.0d (La Jolla, CA). Data represent one biological replicate for each microsome source.

Figure 3. MDA-MB-231 cell death correlates with predicted 4OHCP exposure *in vitro*.
A. Cytotoxicity in MDA-MB-231 cells following 4OHCP treatment. MDA-MB-231 cells were treated with 4OHCP by metabolic activation of CP, with each of the listed microsomes, on top of the cells and subsequent cytotoxicity was monitored as described. All cell/microsome combinations were treated with the same concentrations of CP except for the human and cat microsomes which were treated with two higher concentrations (2874 and 3831 μM). Points and bars represent mean and standard deviation, respectively, from three independent replicates, each with three technical replicates. B. Correlation between MDA-MB-231 cytotoxicity and predicted 4OHCP exposure. 4OHCP exposure was calculated as AUC for each experiment at each concentration as described in the methods. Points represent means from the cytotoxicity curves shown in (a) but without error bars. For each species, Spearman correlation and two-tailed p-value were calculated with GraphPad Prism v7.0d.

Figure 4. Relative abundance of microsomal CYP2B and the contribution of CYPs to 4OHCP formation.
A. Representative immunoblot against CYP2B orthologs in the listed microsomes. The molecular markers, provided for reference on the left and separated from the blot by a black line, is a separate image exposure of the same blot with which it is associated. B. Spearman

correlation between relative CYP2B density and apparent V_{max} for each immunoblotted microsome. Densities were estimated as described in the methods. Briefly, density was calculated as CYP2B pixel intensity divided by the total protein pixel intensity. Points represent the mean of three separate densitometry calculations (Supplemental Table 4). Spearman correlation and two-tailed p-value were calculated with GraphPad Prism v7.0d. C. Effect of CYP inhibitors on 4OHCP formation. Microsomes H1, D4, C2, and M3 were tested with a variety of CYP inhibitors at a single initial CP concentration and 4OHCP concentration was quantified over a 120 minute period. AUC of 4OHCP concentration vs. time curves for each microsome were calculated and normalized to the +CP positive control. Bars represent normalized AUC of one time course experiment for each condition.

Figure 5. Diagram of the semi-physiologic model used to simulate CP pharmacokinetics *in vivo*. CP delivery was modeled as IV bolus or infusion, depending on the study being simulated. Distribution from the plasma to the liver and remaining body was modeled based on species-specific cardiac output and fraction of that cardiac output delivered to the tissue. The single route of elimination for CP was modeled as metabolism into 4OHCP occurring only in the liver based on the Michaelis-Menten parameters observed for each species. *In vitro* microsome K_m and V_{max} values were scaled by reported liver volume and microsomal protein per gram of liver for each species, referenced in Table 3 and Equation 1.

Figure 6. Comparison of animal CP plasma PK data to simulated CP concentration using a semi-physiologic model.

A semi-physiologic model describing the metabolism of CP was generated and used to simulate CP PK using each of the listed microsome's kinetics parameters. Simulation output, in colored lines, is compared to published PK data for (a) dogs (Warry et al., 2011), (b) cats (Stroda et al., 2017), and (c) mice (Supplemental Figure 4), where each symbol represents plasma CP concentrations from one animal subject.

Figure 7. Comparison of human CP plasma PK data to simulated CP concentration using a semi-physiologic model.

A semi-physiologic model describing the human metabolism of CP was generated and used to simulate CP PK using the kinetics parameters from H1, H2, and H3. Model output is represented as the simulated mean (solid lines) ± standard deviation (filled area to dotted lines) compared against two sets of published CP PK data, (a) (Struck et al., 1987) and (b) (Chen et al., 1995), where each symbol represents plasma CP concentrations from one patient. Dosing was modeled as (a) IV bolus or (b) 90-minute IV infusion.

TABLES

Table 1. Source information for each batch of microsomes used in the study.

ID	Species	Production	Lot/Batch	Sex	Age	Pool Size
H1	Human	XenoTech (H0620)	1610016	Mixed	Mixed	50
H2	Human	Corning (452161)	6123001	Mixed	Mixed	33
H3	Human	Gibco (HMMCPL)	PL050B	Mixed	Mixed	50
D1[a]	Canine, Labrador	Lab-Made		Female	2 years	4
D2[b]	Canine, Labrador	Lab-Made		Male	14 years	1
D3[a]	Canine, Hound	Lab-Made		Female	10 months	5
D4	Canine, Beagle	XenoTech (D1500)	1310105	Female	Mixed (4-9 years)	12
C1[b]	Feline, Mixed Breed	Lab-Made		Mixed	Mixed	4
C2	Feline, Short Hair	XenoTech (F1000)	0610343	Male	Sexually Mature	3
M1[a]	Mouse, NIH CD1 Swiss	Lab-Made		Female	6 weeks	5
M2[a]	Mouse, NIH CD1 Swiss	Lab-Made		Female	Mixed	3
M3	Mouse, NIH CD1 Swiss	XenoTech (M1500)	1410027	Female	Mixed	990

[a]Microsomes were prepared immediately from freshly-harvested liver samples.

[b]Microsomes were prepared from liver samples that were frozen upon receipt.

DMD Fast Forward. Published on December 19, 2018 as DOI: 10.1124/dmd.118.083766
This article has not been copyedited and formatted. The final version may differ from this version.

Table 2. Michaelis-Menten kinetics parameters and clearance estimates for each source of microsomes.

The data are listed as the parameter estimate ± standard error of the curve fit[a] and are based on *n = 1* biological replicate.

Species	ID	V_{max} (pmol 4OHCP/min/mg)	K_M (μM)	CL_{int} (V_{max}/K_M) (μL/min^{-1}*mg^{-1})
Human	H1	3372 ± 193.8	2908 ± 463.5	1.160
	H2	2238 ± 333.8	3906 ± 1453	0.5730
	H3	2214 ± 310.5	6631 ± 1865	0.3339
Dog	D1	4633 ± 173.3	66.08 ± 4.186	70.11
	D2	4803 ± 159.9	259.1 ± 13.38	18.54
	D3	5707 ± 236.5	135.6 ± 11.07	42.09
	D4	3862 ± 393.1	182.0 ± 33.79	21.22
Cat	C1	646.7 ± 15.68	84.09 ± 6.223	7.691
	C2	668.0 ± 16.00	34.33 ± 2.518	19.46
Mouse	M1	8577 ± 468.7	156.4 ± 16.23	54.84
	M2	3278 ± 260.4	156.3 ± 23.79	20.97
	M3	4859 ± 485.4	239.9 ± 39.69	20.25

[a]Goodness-of-fit from nonlinear regression for each collection of microsomes is as follows: Human, $R^2_{adj} > 0.90$; Dog, $R^2_{adj} > 0.98$; Cat, $R^2_{adj} > 0.99$; and Mouse, $R^2_{adj} > 0.99$.

Table 3. Physiologic parameters used to construct semi-physiologic model.

		Human	Dog	Cat	Mouse
	Bodyweight (kg) [a]	70	25	4	0.02
Fraction of Bodyweight	Blood[a]	0.079	0.082	0.08	0.049
	Liver[a]	0.0257	0.0329	0.0329	0.055
	Remaining	0.8953	0.8851	0.8871	0.896
	Cardiac Output (mL/min) [b]	$6.66x10^3$	$3.07x10^3$	777.8175	14.6253
Fraction of Cardiac Output	Liver[a]	0.227	0.297	0.202	0.161
	Remaining	0.773	0.703	0.798	0.839
	Microsomal Protein (mg protein/g liver)	50[c]	55[e]	48[f]	87[d]

[a](Brown et al., 1997)

[b]Cardiac output parameter calculated by allometric scaling.

[c](Carlile et al., 2001, Barter et al., 2007)

[d](Gibhard et al., 2016)

[e](Smith et al., 2008)

[f](Visser et al., 2018)

Table 4. Noncompartmental analysis comparisons between actual CP PK data vs. semi-physiologic simulation predicted CP PK data.

Data for AUC and $t_{1/2}$ are presented as mean and standard deviation (S.D.). Units are as follows: AUC (mM * hour); $t_{1/2}$ (hour); Dose (mg/kg).

		AUC (mean)	AUC (S.D.)	Ratio (sim/actual)	$t_{1/2}$ (mean)	$t_{1/2}$ (S.D.)	Ratio (sim/actual)	Dose (mean)	Dose (S.D.)
Human (Struck et al., 1987)	Actual	48.84	2.17		4.92	0.11		27	0
	Averaged	38.42		0.79	5.64		1.15	27	
	1	23.82		0.49	2.84		0.58	27	
	2	37.47		0.77	4.42		0.90	27	
	3	53.98		1.11	6.67		1.35	27	
Human (Chen et al., 1995)	Actual	261.53	47.41		3.53	0.67		108	
	Averaged	152.58		0.58	5.62		1.60	108	
	1	94.783		0.36	2.84		0.81	108	
	2	148.48		0.57	4.44		1.26	108	

		214.4							
	3	9		0.82	6.70		1.90	108	
Dog	Actual	1.64	0.87		0.78	0.38		11.8	1.46
	Average								
	d	1.75		1.07	0.85		1.09	12	
	1	1.72		1.05	0.84		1.08	12	
	2	1.78		1.09	0.87		1.11	12	
	3	1.73		1.06	0.85		1.08	12	
	4	1.77		1.08	0.86		1.10	12	
Cat	Actual	2.06	1.76		0.59	0.24		8.02	1
	Average								
	d	2.87		1.39	0.80		1.38	8	
	1	3.03		1.47	0.84		1.44	8	
	2	2.70		1.31	0.77		1.31	8	
Mous									
e	Actual	4.09	0.88		0.19	0.01		100	0
	Average								
	d	9.61		2.35	0.23		1.21	100	
	1	9.46		2.32	0.22		1.19	100	
	2	9.78		2.40	0.23		1.22	100	
	3	9.76		2.39	0.23		1.23	100	

DMD Fast Forward. Published on December 19, 2018 as DOI: 10.1124/dmd.118.083766
This article has not been copyedited and formatted. The final version may differ from this version.

FIGURES

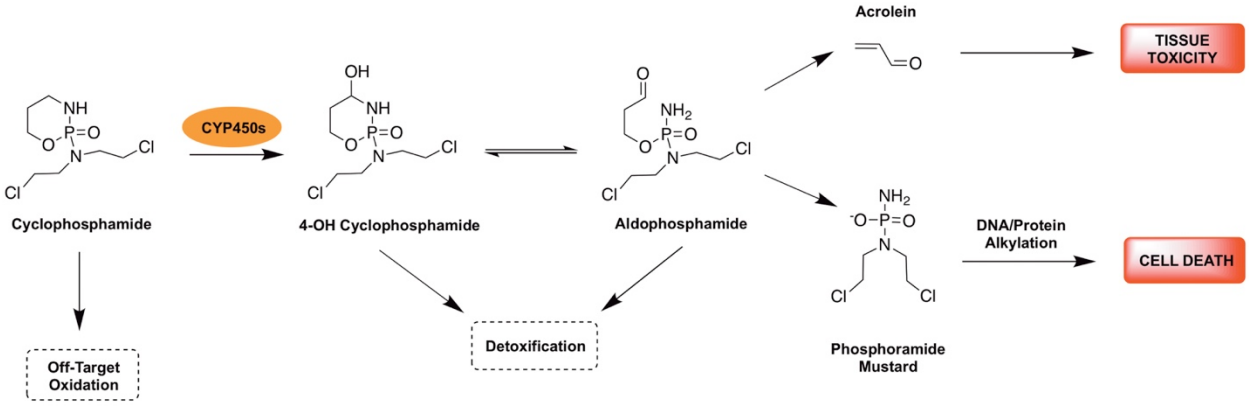

Figure 1.

DMD Fast Forward. Published on December 19, 2018 as DOI: 10.1124/dmd.118.083766
This article has not been copyedited and formatted. The final version may differ from this version.

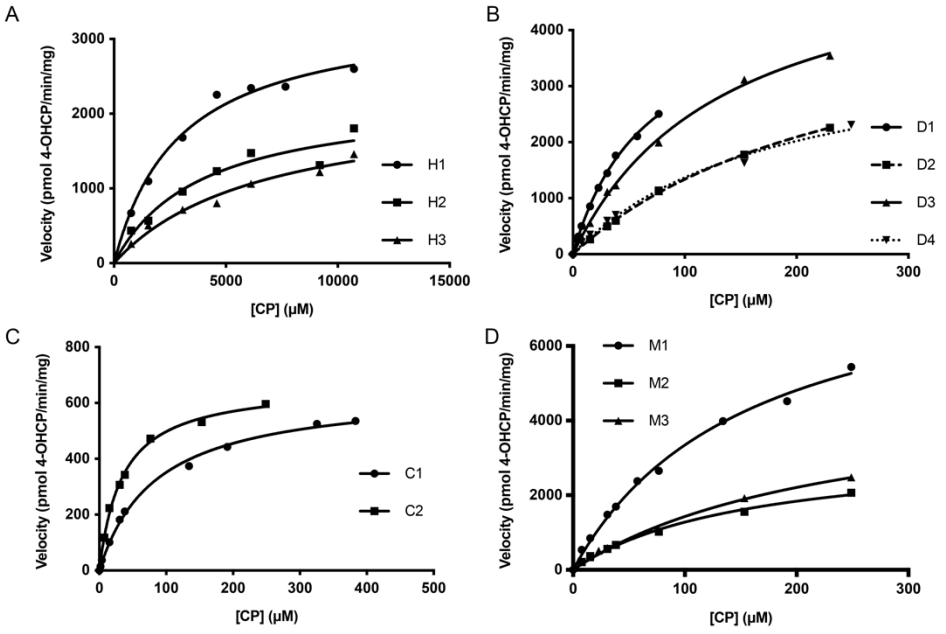

Figure 2.

DMD Fast Forward. Published on December 19, 2018 as DOI: 10.1124/dmd.118.083766
This article has not been copyedited and formatted. The final version may differ from this version.

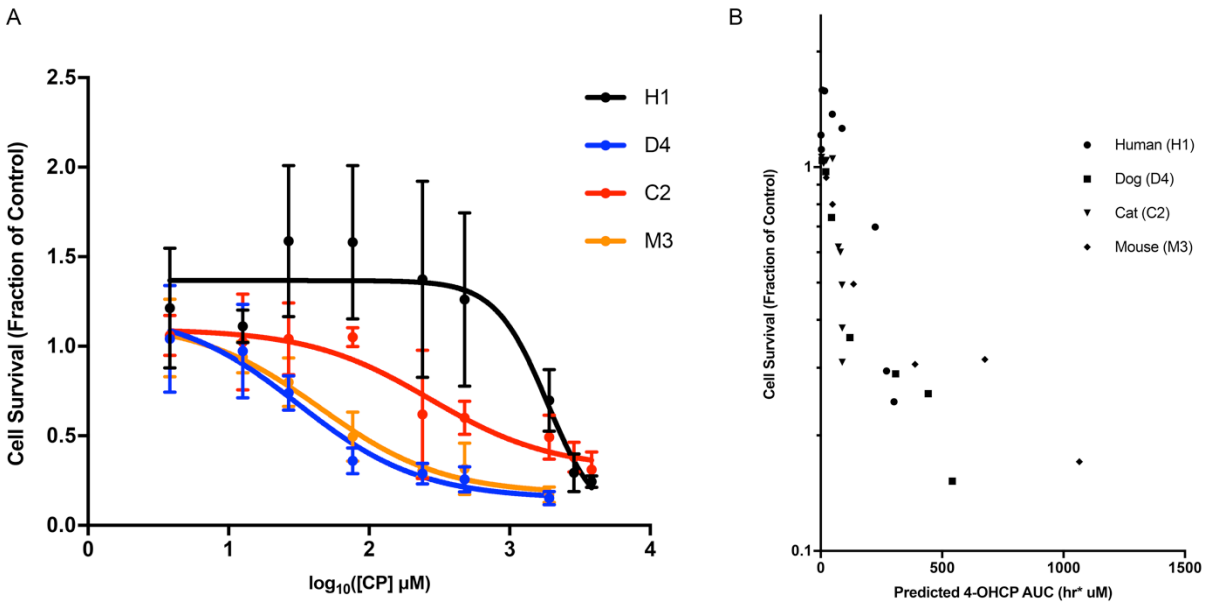

Figure 3.

DMD Fast Forward. Published on December 19, 2018 as DOI: 10.1124/dmd.118.083766
This article has not been copyedited and formatted. The final version may differ from this version.

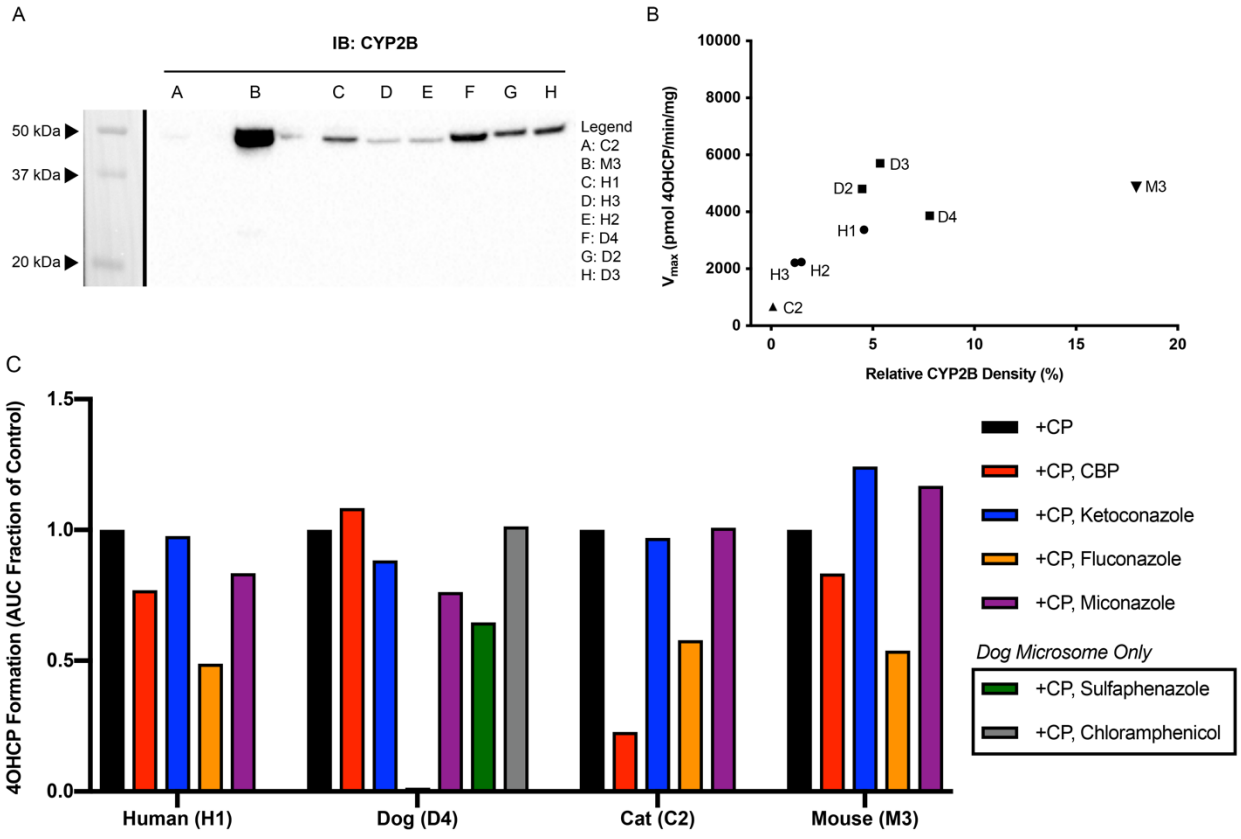

Figure 4.

DMD Fast Forward. Published on December 19, 2018 as DOI: 10.1124/dmd.118.083766
This article has not been copyedited and formatted. The final version may differ from this version.

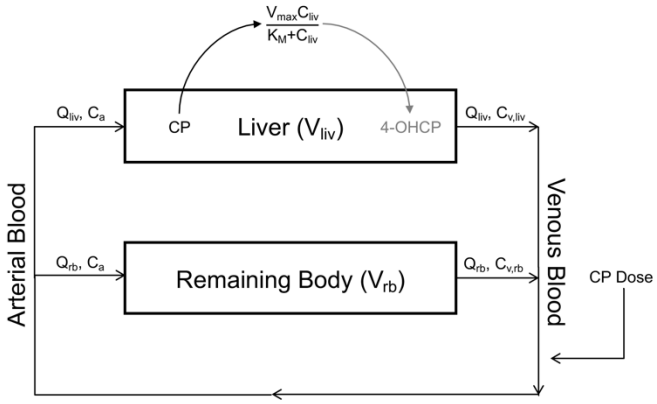

Figure 5.

DMD Fast Forward. Published on December 19, 2018 as DOI: 10.1124/dmd.118.083766
This article has not been copyedited and formatted. The final version may differ from this version.

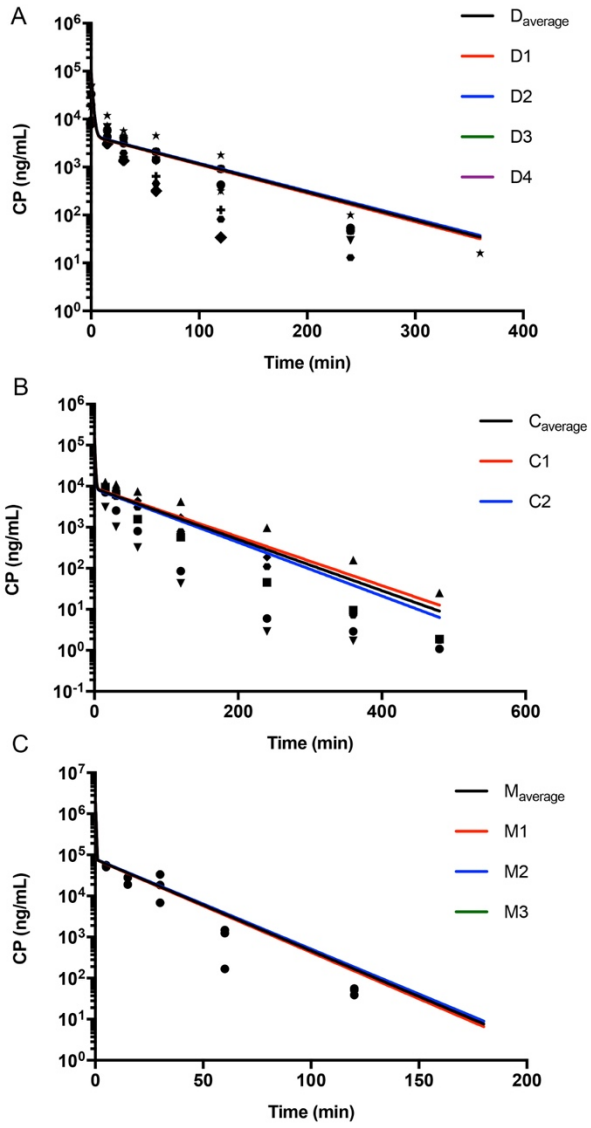

Figure 6.

DMD Fast Forward. Published on December 19, 2018 as DOI: 10.1124/dmd.118.083766
This article has not been copyedited and formatted. The final version may differ from this version.

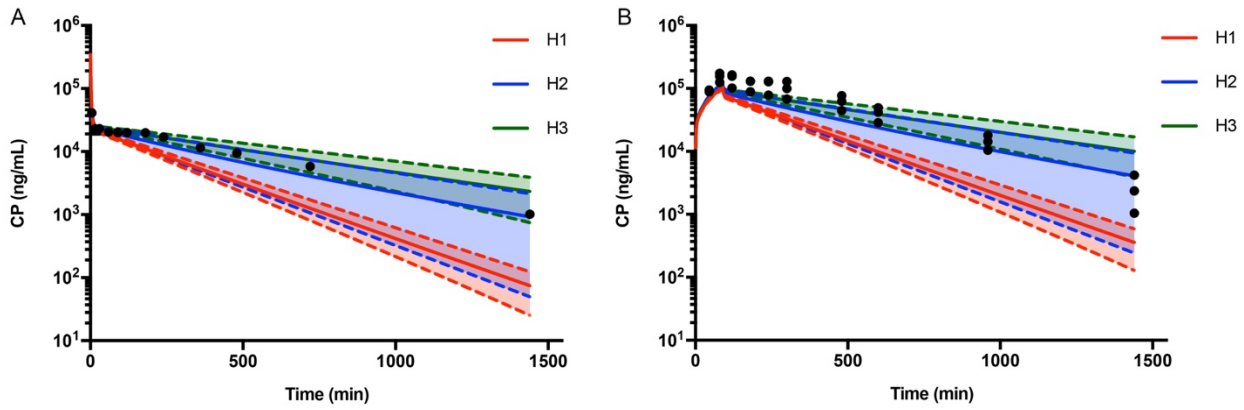

Figure 7.